THE JOURNAL OF PHYSICAL CHEMISTRY Letters

Letter

pubs.acs.org/JPCL

Static and Dynamic Energetic Disorders in the C_{60}, $PC_{61}BM$, C_{70}, and $PC_{71}BM$ Fullerenes

Naga Rajesh Tummala,*[,†] Zilong Zheng,[†] Saadullah G. Aziz,[‡] Veaceslav Coropceanu,*[,†] and Jean-Luc Brédas*[,§]

[†]School of Chemistry and Biochemistry & Center for Organic Photonics and Electronics, Georgia Institute of Technology, Atlanta, Georgia 30332-0400, United States

[‡]Department of Chemistry, King Abdulaziz University, Jeddah 21589, Kingdom of Saudi Arabia

[§]Solar and Photovoltaics Engineering Research Center, Division of Physical Science and Engineering, King Abdullah University of Science and Technology, Thuwal 23955-6900, Kingdom of Saudi Arabia

Supporting Information

ABSTRACT: We use a combination of molecular dynamics simulations and density functional theory calculations to investigate the energetic disorder in fullerene systems. We show that the energetic disorder evaluated from an ensemble average contains contributions of both static origin (time-independent, due to loose packing) and dynamic origin (time-dependent, due to electron-vibration interactions). In order to differentiate between these two contributions, we compare the results obtained from an ensemble average approach with those derived from a time average approach. It is found that in both amorphous C_{60} and C_{70} bulk systems, the degrees of static and dynamic disorder are comparable, while in the amorphous $PC_{61}BM$ and $PC_{71}BM$ systems, static disorder is about twice as large as dynamic disorder.

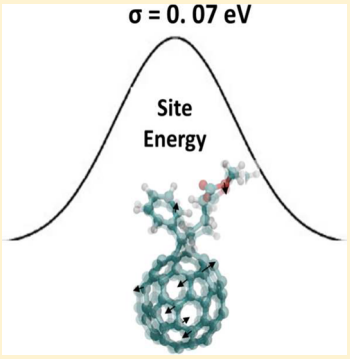

Organic molecular semiconductors are currently of interest for many applications such as field-effect transistors, photovoltaic cells, or light-emitting diodes.[1−6] In most instances, the efficiency of these devices strongly depends on the charge-transport properties of the active organic layer. In spite of extensive efforts over several decades, reaching a complete understanding of the charge-transport mechanism in organic semiconductors remains a challenge.[7−12]

Organic thin-film electronic devices generally suffer from the presence of significant structural disorder and chemical defects. While disorder is especially significant in the case of amorphous materials, it should be borne in mind that a sizable density of trap states ($\sim 10^{15}-10^{18}$ cm^{-3}) is found to be present even in the case of high-mobility organic single crystals such as rubrene and pentacene.[13−17] Therefore, it is important to keep developing experimental and theoretical approaches to better estimate the amount of disorder in organic materials as well as to understand its nature and how it affects the electrical properties.[7]

When discussing the role of disorder, the distinction must be made between dynamic disorder and static disorder. The former is related to electron−vibration (phonon) interactions that result in a time-dependent variation of the microscopic transport parameters, i.e., of the site energies and transfer integrals (electronic couplings). In the absence of chemical and physical defects, in a perfectly ordered crystalline system, the dynamic disorder is the only type of disorder present. However, as a system departs from a crystalline structure and loses translational symmetry, both site energies and transfer integrals span a whole range of values even when vibrational motions are neglected; these distributions of site energies and transfer integrals, which are time-independent, are referred to as energetic static disorder and positional static disorder, respectively. The dynamic and static disorders both affect the charge-transport properties but in rather different ways. For instance, in the case of large transfer integrals, a weak static disorder leads to localization of the electronic states in the band tails, while weak electron-vibration couplings result in transitions between band states.[8] Interestingly, while static disorder is always detrimental for charge transport, dynamic disorder can in some instances lead to an enhancement of the transport properties via a phonon-assisted contribution to charge-carrier mobility.[7,18,19] In the case of weak electronic couplings (i.e., when charge transport can be reliably described by a hopping mechanism) and in the context of a semiclassical Marcus electron transfer model, the static disorder can be accounted for by assuming distributions in site energies (energetic disorder) and transfer integrals (positional disorder) while the dynamic disorder can be characterized through the reorganization energy (which provides an overall measure of the electron-vibration couplings).[7,9]

Received: August 6, 2015
Accepted: September 2, 2015
Published: September 2, 2015

DOI: 10.1021/acs.jpclett.5b01709
J. Phys. Chem. Lett. 2015, 6, 3657−3662

Several theoretical groups have recently addressed the static disorder issue in amorphous and partially disordered materials.[20−24] Usually, a two-step approach is considered: In the first step, temperature equilibrated morphologies are generated by means of molecular dynamics (using empirical force-field calculations) simulations; in the second step, the positional and energetic disorders are derived by using a quantum-mechanical (QM) approach to compute the distribution of transfer integrals and by using as well a QM approach or a combination of QM and, for instance, an electrostatic approach to compute the distribution of site energies. We note, however, that morphologies created by means of atomistic molecular dynamics simulations (MD) contain both a static disorder contribution resulting from the presence of translationally nonequivalent molecules in the generated supercells (compared to the case of the ordered morphology, i.e., the global minimum) *and* a contribution due to dynamic fluctuations of the atoms around the local equilibrium positions. Therefore, the disorder estimated by means of such computational approaches is not a true measure of the static disorder as is customarily assumed in the current literature. It must be realized that, in reality, it contains the contributions from both static and dynamic mechanisms. To the best of our knowledge, the issue of separating these two contributions has not been addressed to date.

Here, we discuss how the change in molecular packing when going from a crystalline structure to an amorphous structure affects the static and dynamic energetic disorders. We have chosen to focus on C_{60}, C_{70}, $PC_{61}BM$ (phenyl-C_{61}-butyric acid methyl ester), and $PC_{71}BM$ (phenyl-C_{71}-butyric acid methyl ester), i.e., systems of high current interest in organic electronics.

Within the linear electron−vibration approximation, the site energy can be written as[25,26]

$$\varepsilon = \varepsilon^0 + \sum_j \nu_j Q_j + \ldots \tag{1}$$

Here, ε^0 is the site energy at the equilibrium geometry, and ν_j denotes the electron−vibration coupling constant due to vibrational mode Q_j. The static energetic disorder is given by the distribution of the ε^0 site energies and the second term in eq 1 is responsible for the dynamic disorder. The mean site energy and its variance, within the harmonic approximation eq 2 and in the absence of static disorder, are given by eq 3 and eq 4, respectively:

$$H = \frac{1}{2}\sum_j \hbar\omega_j (P_j^2 + Q_j^2) \tag{2}$$

$$\langle\varepsilon\rangle = \varepsilon^0 \tag{3}$$

$$\sigma^2 = \sum_j \frac{\varepsilon_j^2}{2} \coth\frac{\hbar\omega_j}{2k_BT} \tag{4}$$

where ω_j, and P_j denote the frequency and momentum of vibrational mode Q_j. In the limit of high temperatures, i.e., when the vibrations can be treated classically, eq 4 takes the form

$$\sigma^2 = \sum_j \frac{\varepsilon_j^2 k_BT}{\hbar\omega_j} = 2\lambda_{rel}k_BT \tag{5}$$

Here, λ_{rel} denotes the relaxation energy that provides an overall measure of the electron−vibration interactions. Equation 5 will be used below to estimate λ_{rel} (we note that the reorganization energy in Marcus electron-transfer theory corresponds to twice λ_{rel}); alternatively, λ_{rel} can be derived from the adiabatic potential energy surfaces of the neutral and charged states of the molecule (see Figure S1 in the Supporting Information (SI) for details).

The structures of the amorphous $PC_{61}BM$ and $PC_{71}BM$ and crystalline $PC_{61}BM$ systems were taken from our previous work.[27,28] The amorphous bulk structures of C_{60} and C_{70} were derived in a way similar to those of $PC_{61}BM$ and $PC_{71}BM$[27] by performing MD simulations with the GROMACS software package.[29,30] As in our previous work, the OPLS-AA (optimized parameters for liquid simulations-all atom) force field[31] was used to describe the bonded and nonbonded interactions. Our recent results indicate that this procedure and force field provide densities and solubility parameters that compare well to experimental data.[32,33] In order to understand the role of phenyl-butyric acid methyl ester adducts on the dynamic and static disorders, we also considered the crystalline triclinic structure of $PC_{61}BM$ in which the $PC_{61}BM$ molecules were replaced by C_{60} fullerene cages.

In the case of electron transport, the site energy ε_i is defined as the electron affinity of the system, i.e., its affinity with respect to an excess electron becoming localized on molecule *i*. Here, in order to speed up the calculations, we applied Koopmans' Theorem and approximated the site energy via the energy of the highest occupied molecular orbital (HOMO) of the *anion* state. The site energies were computed at the density functional theory (DFT) level using the tuned range-separated hybrid functional, ωB97XD[34,35] functional, and the 6-31G(d,p) basis set. This approach was shown earlier to accurately describe the energy levels of π-conjugated molecules.[36,37] The range-separation parameter (ω) was optimized (tuned) using a nonempirical procedure (see SI for details).[37] In order to account for the environment effect, 200 clusters containing molecules within a radius of 1.2 nm from the reference molecule have been considered. Subsequently, iterative QM calculations on each molecule in the presence of point charges on the atoms of the neighboring molecules are performed. The point charges around the central molecule play a significant role in the correct description of the orbital energies due to the induced electronic polarization. We used the Charge Model 5 (CM5) methodology[38] to extract the point charges from the DFT calculations, as this model has been shown to suffer the least from the choice of the functional and basis set.[39] In the first iteration, the point charges obtained from a DFT calculation on the isolated molecule are used. Iterations are then performed until the energy of the central molecule in the presence of point charges converges to $<10^{-4}$ atomic units (<2.7 meV), which generally occurs after 4−5 iterations. The resulting convergence of point charges is much smaller than 0.01 *e*, a value sometimes used as a convergence criterion in such types of studies. The molecular geometries are kept constant during the iterative procedure. The mean value of the site-energy distribution and its standard deviation are calculated using eqs 6 and 7, respectively:

$$\langle\varepsilon\rangle = \frac{\sum_{i=1}^{N}\varepsilon_i}{N} \tag{6}$$

DOI: 10.1021/acs.jpclett.5b01709
J. Phys. Chem. Lett. 2015, 6, 3657−3662

$$\sigma = \sqrt{\frac{\sum_{i=1}^{N} (\varepsilon_i - \langle \varepsilon \rangle)^2}{N - 1}} \quad (7)$$

where N is the number of clusters considered.

The relaxation energies were also calculated directly from the relevant points on the potential energy surfaces (see Figure S1) using the common procedure detailed in the literature.[40] These calculations were performed using both ωB97XD and B3LYP functionals and the 6-31G(d,p) basis set. The Gaussian-09D package was used for all DFT calculations.[41]

In order to estimate the dynamic disorder in the case of an *isolated* molecule, we carried out MD simulations based on very large unit cells (at least 5 nm long in any dimension), each containing a single molecule. The molecular coordinates were saved every 50 fs; at least 200 configurations were used in the statistical analysis and subsequently to derive the relaxation energy. Figure 1 displays the distribution probability of the

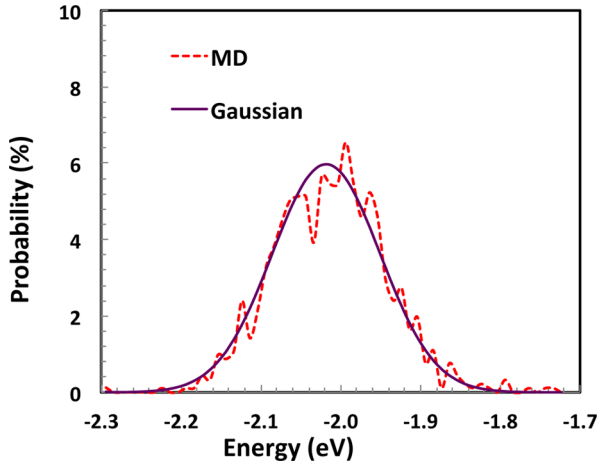

Figure 1. Distribution probability of the electron site energy of the isolated $PC_{61}BM$ molecule derived from the combination of QM/MD simulations at room temperature. A Gaussian-type probability distribution is generated using the QM/MD-derived mean value and standard deviation.

electron site energies for an isolated $PC_{61}BM$ molecule, derived at room temperature, along with the corresponding Gaussian-type distribution based on the QM/MD-derived mean value and standard deviation; the results for the other systems are given in the SI (Figure S2 and Table S1). If we take the example of the individual C_{60} and $PC_{61}BM$ molecules, it is of interest to realize that the dynamic disorder at room temperature induces a Gaussian-type distribution in site energies with a fwhm (full width at half-maximum) on the order of 0.13 eV (standard deviation σ = 0.06 eV) for C_{60}, which increases to 0.18 eV (σ = 0.08 eV) for $PC_{61}BM$, *vide infra*. The temperature dependence of the calculated distribution variance is shown in Figure 2 (see also Figure S3); the observed linear dependence indicates that eq 5 can be used reliably to estimate the relaxation energy.

The QM/MD calculations yield, following eq 5, a value of 0.087 eV (slope of the line in Figure 2) for the relaxation energy λ_{rel} of $PC_{61}BM$; this value compares very well with the DFT value of 0.089 eV obtained from the adiabatic potential energy surface of the $PC_{61}BM$ anion state (see Table 1), computed at the same ωB97XD/6-31G(d,p) level of calculation. We note that this ωB97XD estimate is about

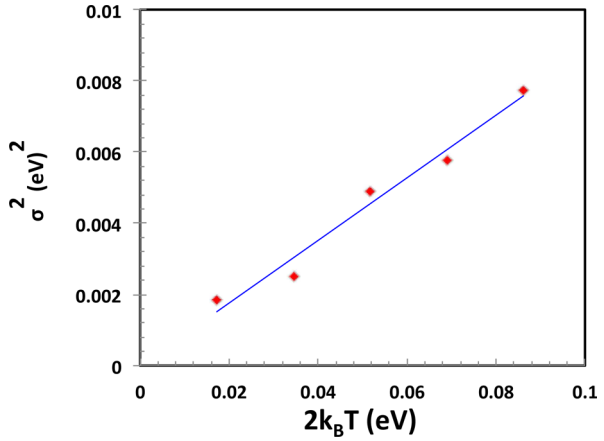

Figure 2. Temperature dependence of the distribution variance of the electron site energy for an isolated $PC_{61}BM$ molecule.

Table 1. Relaxation Energy (in eV) of the Various Fullerene Systems Derived from the Adiabatic Potential Energies of the Radical-Anion States

	ωB97XD		B3LYP
	ω	λ_{rel}	λ_{rel}
C_{60}	0.178	0.084	0.069
C_{70}	0.184	0.202	0.064
$PC_{61}BM$	0.147	0.089	0.077
$PC_{71}BM$	0.135	0.230	0.100

16% larger than the B3LYP value, see Table 1; a similar result (21% larger) is also obtained for C_{60} (these differences are somewhat smaller than what was previously found in the case of the hole reorganization energies in oligoacenes, where the values derived by means of tuned range-separated functionals are about 30% larger than those from B3LYP calculations).[42] In comparison to C_{60} and $PC_{61}BM$, the ωB97XD-calculated values of λ_{rel} for C_{70} and $PC_{71}BM$ are significantly larger, 0.202 and 0.230 eV, respectively. These values are twice as large as the corresponding B3LYP values; for instance, on going from C_{60} to C_{70}, while the B3LYP relaxation energy slightly decreases from 69 to 64 meV, the trend is opposite at the ωB97XD level and λ_{rel} strongly increases from 84 to 202 meV. Inspection of the frontier molecular orbitals (see Figure S4) shows that the unpaired electron in the C_{60}^- anion is delocalized at both B3LYP and ωB97XD levels while in the C_{70}^- anion the unpaired electron remains delocalized at the B3LYP level but becomes *localized* at the ωB97XD level. The ωB97XD results are in agreement with a comparison of the vibrational structures of the first ionization peaks of C_{60}^- and C_{70}^- derived by means of photoelectron spectroscopy, which points to a larger relaxation energy in the case of C_{70}^-.[43,44] Overall, this conclusion is consistent with the fact that the electron mobilities in C_{60} and $PC_{61}BM$ thin films are larger than in $PC_{71}BM$.[45] In the context of the present discussion, it is useful to recall that B3LYP has been demonstrated to overdelocalize wave functions, especially in the case of extended π-conjugated systems, a deficiency precisely overcome by tuned long-range corrected functionals.[46] We also note that the normal-mode calculations (see Figure S5) reveal that more than 50% of the dynamic disorder in both C_{60} and C_{70} arises from high-frequency vibrational modes in the range of 1200−1600 cm^{-1}.[47]

DOI: 10.1021/acs.jpclett.5b01709
J. Phys. Chem. Lett. 2015, 6, 3657−3662

We now turn to the bulk structures. In order to differentiate between static and dynamic energetic disorder, we examine the site-energy distributions derived from an ensemble average and from a time average. In the former case, the results obtained for 200 molecular clusters extracted from the MD simulations are used for the statistical analysis. In the latter case, the procedure is similar to the one described above for the isolated molecules; however, here, the first-neighbor shells of 20 different clusters extracted from the equilibrated bulk structures are followed in time and 200 configurations of each cluster are used for the site-energy calculations. In both cases, the site energies are computed following the approach described previously. The results derived for $PC_{61}BM$ are given in Table 2.

Table 2. Standard Deviation, Mean Value, Width ($W = \varepsilon_{max} - \varepsilon_{min}$), and Asymmetry ($A = 2\langle\varepsilon\rangle - \varepsilon_{max} - \varepsilon_{min}$) of the Site Energy Distributions of the $PC_{61}BM$ Fullerene Derivative Derived from Ensemble Average and Time Average Calculations[a]

	σ	$\langle\varepsilon\rangle$	W	A
ensemble average				
$PC_{61}BM$ (triclinic)	0.10	−2.54	0.55	0.01
$PC_{61}BM$ (amorphous)	0.13	−2.48	0.89	−0.25
time average				
$PC_{61}BM$ (triclinic)	0.08	−2.52	0.42	0.00
$PC_{61}BM$ (amorphous)	0.07	−2.42	0.40	0.00

[a]All energies are given in eV. The error bars for σ are 0.01 eV.

Our calculations show that, as a result of electronic polarization effects, the site energy of $PC_{61}BM$ in the solid state is stabilized by about 0.5 eV in comparison to the isolated molecule. Such a stabilization energy is smaller than the value of 1.2 eV estimated via inverse photoemission spectroscopy.[48] The main reason for this discrepancy is expected to be related to the small size of the clusters used in the calculations. Indeed, preliminary results obtained for other fullerene derivatives confirm that by increasing the number of surrounding molecules beyond the first shell around the reference molecule, the stabilization of the site energy increases; importantly, however, σ, which is the main parameter of interest in the present work, hardly changes upon such increase in cluster size.

In the case of the isolated molecule, the σ value in site-energy distribution estimated for $PC_{61}BM$ at room temperature is ca. 0.077 eV. Turning to the bulk crystalline and amorphous structures, the ensemble average approach yields an increase in the σ value by about 0.02 and 0.05 eV, respectively. In contrast, the standard deviations of the distributions derived from a time average approach are *identical*—within the limits of the errors of our methodology—to that derived for the isolated molecule. This finding that the dynamic energetic disorder is equivalent in isolated molecules and in the bulk, is in fact not surprising; indeed, previous studies have shown that, in the case of organic molecular crystals, the main contribution to the relaxation energy is due to electron interactions with *intramolecular* vibrations, which are usually only slightly affected by *intermolecular* interactions in the bulk.[26] We note that this is also the reason why an increase in the cluster size affects the site energy but not the width of the site-energy distribution.

The parameters reported in Table 2 from the time average approach are obtained by an additional averaging over all 20 clusters that have been considered in the time-dependent calculations. However, if the sets of mean values of the reference sites are considered, then they form a distribution resembling the distribution derived from the ensemble average calculations; this result is illustrated in Figure 3. Thus, we come

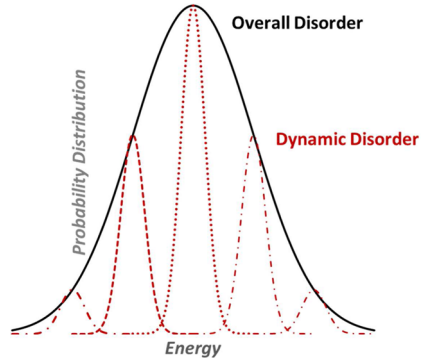

Figure 3. Schematic illustration of the dynamic contribution to the total site-energy disorder in an amorphous molecular structure. The dashed, dotted, and dashed-dotted lines represent the dynamic disorder of various sites within the ensemble.

to the important conclusion that the distribution derived from the ensemble average can be considered as arising from the convolution of *two* distributions related to static and dynamic energetic disorders. Assuming that both distributions are Gaussian-like, then the variance of the distribution derived from the ensemble average (σ_T^2) can be expressed via the corresponding variances of the static disorder (σ_S^2) and dynamic disorder (σ_D^2) as

$$\sigma_T^2 = \sigma_S^2 + \sigma_D^2$$

By applying this relationship and using the parameters derived from the ensemble average and time average calculations, the standard deviations of the static disorder in crystalline and amorphous structures of $PC_{61}BM$ are estimated to be 0.06 and 0.11 eV, respectively. The presence of moderate static disorder even in the MD-generated (triclinic) crystalline structures of $PC_{61}BM$ can be rationalized by the fact that while the $PC_{61}BM$ molecular centers of masses form a regular crystalline lattice, there remains some structural disorder along the rotational degrees of freedom and those of the phenyl-butyric acid methyl ester adducts.

The computed σ_S values for the fullerenes investigated here are shown in Table 3. Here, the dynamic disorder parameters have been taken from the MD simulations on the isolated molecules (Table S1). Also, for the sake of comparison, the DFT calculations for these systems have been performed with

Table 3. Standard Deviations of the Total Disorder (σ_T), Dynamic Disorder (σ_D), and Static Disorder (σ_S) Derived for Bulk Structures of C_{60}, $PC_{61}BM$, C_{70}, and $PC_{71}BM$[a]

	σ_T	σ_D	σ_S
C_{60} (amorphous)	0.08	0.06	0.05
C_{60} (triclinic)	0.06	0.06	0.00
$PC_{61}BM$ (amorphous)	0.13	0.07	0.11
$PC_{61}BM$ (triclinic)	0.10	0.08	0.06
C_{70} (amorphous)	0.11	0.08	0.07
$PC_{71}BM$ (amorphous)	0.18	0.09	0.16

[a]All energies are given in eV.

DOI: 10.1021/acs.jpclett.5b01709
J. Phys. Chem. Lett. 2015, 6, 3657−3662

the ωB97XD functional using the range-separated parameter ω optimized for $PC_{61}BM$.

The results indicate that

(i) the static disorder in the amorphous systems increases by about 40% when going from C_{60} to C_{70} and from $PC_{61}BM$ to $PC_{71}BM$;
(ii) the static disorder and dynamic disorder have comparable magnitudes in amorphous C_{60} and C_{70} structures; and
(iii) the static disorder is more than doubled for the PCBM analogs of the fullerenes; visual inspection of the MD trajectories show that the phenyl-butyric acid methyl ester adducts undergo more conformational changes than the fullerene cages and therefore significantly contribute to the static disorder.

Using a combined density functional theory and molecular dynamics approach, we have investigated the specific contributions of dynamic disorder and static disorder to the overall energetic disorder in C_{60}, C_{70}, $PC_{61}BM$, and $PC_{71}BM$ as the system evolves from the isolated molecule to bulk crystalline and amorphous structures.

The dynamic energetic disorder at room temperature is calculated to be very similar in the isolated molecules versus the bulk systems, which confirms that the dynamic disorder is primarily driven by electron interactions with intramolecular vibrations. For the C_{60}, C_{70}, $PC_{61}BM$, and $PC_{71}BM$ bulk systems we considered, the standard deviation in site energies due to dynamic disorder ranges from 0.06 to 0.09 eV and shows only a modest increase when going from unsubstituted to substituted systems.

In the C_{60} and C_{70} bulk amorphous structures, the extent of static disorder is comparable to that of dynamic disorder. However, in the case of the amorphous $PC_{61}BM$ and $PC_{71}BM$ systems, the static disorder increases very significantly and becomes about twice as large as the dynamic disorder. This increase is directly related to the conformational changes coming from the phenyl-butyric acid methyl ester adducts.

Our results also underline that the disorder parameters evaluated on the basis of an ensemble average approach contain both the static and dynamic components. Thus, parameters derived from an ensemble average approach should not be taken as a measure of the static disorder, as is often done in the literature. This is particularly important in the case of highly ordered systems where disorder is dominated by the dynamic component arising from electron−vibration (phonon) couplings.

■ ASSOCIATED CONTENT

Supporting Information

The Supporting Information is available free of charge on the ACS Publications website at DOI: 10.1021/acs.jpclett.5b01709.

The adiabatic potential energy surfaces and the definition for relaxation energies; the equation used to optimize ω for tuned long-range hybrid functional; the probability distribution of site energies in C_{60} and $PC_{61}BM$; the disorder versus temperature plots for C_{60} and $PC_{61}BM$; the relaxation energies in neutral fullerenes from DFT calculations with optimized ω; the relaxation energies for the neutral and anion states of fullerenes computed with the DFT using ωB97XD functional with ω = 0.147 from the MD derived trajectories; contribution of the vibrational modes to the relaxation energy of C_{60} and C_{70}; and the HOMO orbital pictures of C_{60}^- and C_{70}^- obtained with the ωB97XD and B3LYP functionals. (PDF)

■ AUTHOR INFORMATION

Corresponding Authors

*E-mail: nagarajesh@gatech.edu.
*E-mail: coropceanu@gatech.edu.
*E-mail: jean-luc.bredas@kaust.edu.sa.

Notes

The authors declare no competing financial interest.

■ ACKNOWLEDGMENTS

We gratefully acknowledge the financial support for this work at the Georgia Institute of Technology by the Deanship of Scientific Research of King Abdulaziz University under an International Collaboration Grant (Award No. D-001-433), by the Department of the Navy, Office of Naval Research (Award No. N00014-14-1-0580), and by King Abdullah University of Science and Technology (V.C.). The work at King Abdullah University of Science and Technology has been supported by KAUST competitive research funding and by the Office of Naval Research Global (Award No. N62909-15-1-2003).

■ REFERENCES

(1) Mei, J.; Diao, Y.; Appleton, A. L.; Fang, L.; Bao, Z. Integrated Materials Design of Organic Semiconductors for Field-Effect Transistors. *J. Am. Chem. Soc.* **2013**, *135*, 6724−6746.
(2) Mishra, A.; Bäuerle, P. Small Molecule Organic Semiconductors on the Move: Promises for Future Solar Energy Technology. *Angew. Chem., Int. Ed.* **2012**, *51*, 2020−2067.
(3) Bauer, S.; Bauer-Gogonea, S.; Graz, I.; Kaltenbrunner, M.; Keplinger, C.; Schwödiauer, R. 25th Anniversary Article: A Soft Future: From Robots and Sensor Skin to Energy Harvesters. *Adv. Mater.* **2014**, *26*, 149−162.
(4) Tang, C. W.; VanSlyke, S. A. Organic Electroluminescent Diodes. *Appl. Phys. Lett.* **1987**, *51*, 913−915.
(5) Shirakawa, H.; Louis, E. J.; MacDiarmid, A. G.; Chiang, C. K.; Heeger, A. J. Synthesis of Electrically Conducting Organic Polymers: Halogen Derivatives of Polyacetylene, (Ch). *J. Chem. Soc., Chem. Commun.* **1977**, 578−580.
(6) Morel, D. L.; Ghosh, A. K.; Feng, T.; Stogryn, E. L.; Purwin, P. E.; Shaw, R. F.; Fishman, C. High-Efficiency Organic Solar Cells. *Appl. Phys. Lett.* **1978**, *32*, 495−497.
(7) Coropceanu, V.; Cornil, J.; da Silva Filho, D. A.; Olivier, Y.; Silbey, R.; Brédas, J. L. Charge Transport in Organic Semiconductors. *Chem. Rev.* **2007**, *107*, 926−952.
(8) Coropceanu, V.; Li, Y.; Yi, Y. P.; Zhu, L. Y.; Bredas, J. L. Intrinsic Charge Transport in Single Crystals of Organic Molecular Semiconductors: A Theoretical Perspective. *MRS Bull.* **2013**, *38*, 57−64.
(9) Bassler, H.; Kohler, A. Charge Transport in Organic Semiconductors. *Top. Curr. Chem.* **2011**, *312*, 1−65.
(10) Troisi, A. Charge Transport in High Mobility Molecular Semiconductors: Classical Models and New Theories. *Chem. Soc. Rev.* **2011**, *40*, 2347−2358.
(11) Ortmann, F.; Bechstedt, F.; Hannewald, K. Charge Transport in Organic Crystals: Theory and Modelling. *Phys. Status Solidi B* **2011**, *248*, 511−525.
(12) Wang, L. J.; Nan, G. J.; Yang, X. D.; Peng, Q.; Li, Q. K.; Shuai, Z. G. Computational Methods for Design of Organic Materials with High Charge Mobility. *Chem. Soc. Rev.* **2010**, *39*, 423.
(13) Kalb, W. L.; Haas, S.; Krellner, C.; Mathis, T.; Batlogg, B. Trap Density of States in Small-Molecule Organic Semiconductors: A Quantitative Comparison of Thin-Film Transistors with Single Crystals. *Phys. Rev. B: Condens. Matter Mater. Phys.* **2010**, *81*, 155315.

DOI: 10.1021/acs.jpclett.5b01709
J. Phys. Chem. Lett. 2015, 6, 3657−3662

(14) Kalb, W. L.; Mattenberger, K.; Batlogg, B. Oxygen-Related Traps in Pentacene Thin Films: Energetic Position and Implications for Transistor Performance. *Phys. Rev. B: Condens. Matter Mater. Phys.* **2008**, *78*, 035334.
(15) Krellner, C.; Haas, S.; Goldmann, C.; Pernstich, K. P.; Gundlach, D. J.; Batlogg, B. Density of Bulk Trap States in Organic Semiconductor Crystals: Discrete Levels Induced by Oxygen in Rubrene. *Phys. Rev. B: Condens. Matter Mater. Phys.* **2007**, *75*, 245115.
(16) Dacuna, J.; Xie, W.; Salleo, A. Estimation of the Spatial Distribution of Traps Using Space-Charge-Limited Current Measurements in an Organic Single Crystal. *Phys. Rev. B: Condens. Matter Mater. Phys.* **2012**, *86*, 115202.
(17) Dacuna, J.; Salleo, A. Modeling Space-Charge-Limited Currents in Organic Semiconductors: Extracting Trap Density and Mobility. *Phys. Rev. B: Condens. Matter Mater. Phys.* **2011**, *84*, 195209.
(18) Gosar, P.; Choi, S. I. Linear-Response Theory of Electron Mobility in Molecular Crystals. *Phys. Rev.* **1966**, *150*, 529−538.
(19) Gosar, P.; Vilfan, I. Phonon-Assisted Current in Organic Molecular Crystals. *Mol. Phys.* **1970**, *18*, 49−61.
(20) Friederich, P.; Meded, V.; Symalla, F.; Elstner, M.; Wenzel, W. QM/QM Approach to Model Energy Disorder in Amorphous Organic Semiconductors. *J. Chem. Theory Comput.* **2015**, *11*, 560−567.
(21) Rühle, V.; Lukyanov, A.; May, F.; Schrader, M.; Vehoff, T.; Kirkpatrick, J.; Baumeier, B.; Andrienko, D. Microscopic Simulations of Charge Transport in Disordered Organic Semiconductors. *J. Chem. Theory Comput.* **2011**, *7*, 3335−3345.
(22) Poelking, C.; Tietze, M.; Elschner, C.; Olthof, S.; Hertel, D.; Baumeier, B.; Wurthner, F.; Meerholz, K.; Leo, K.; Andrienko, D. Impact of Mesoscale Order on Open-Circuit Voltage in Organic Solar Cells. *Nat. Mater.* **2015**, *14*, 434−439.
(23) Rühle, V.; Junghans, C.; Lukyanov, A.; Kremer, K.; Andrienko, D. Versatile Object-Oriented Toolkit for Coarse-Graining Applications. *J. Chem. Theory Comput.* **2009**, *5*, 3211−3223.
(24) Yavuz, I.; Martin, B. N.; Park, J.; Houk, K. N. Theoretical Study of the Molecular Ordering, Paracrystallinity, and Charge Mobilities of Oligomers in Different Crystalline Phases. *J. Am. Chem. Soc.* **2015**, *137*, 2856−2866.
(25) Coropceanu, V.; Sánchez-Carrera, R. S.; Paramonov, P.; Day, G. M.; Brédas, J.-L. Interaction of Charge Carriers with Lattice Vibrations in Organic Molecular Semiconductors: Naphthalene as a Case Study. *J. Phys. Chem. C* **2009**, *113*, 4679−4686.
(26) Martinelli, N. G.; Idé, J.; Sánchez-Carrera, R. S.; Coropceanu, V.; Brédas, J.-L.; Ducasse, L.; Castet, F. d. r.; Cornil, J. r. m.; Beljonne, D. Influence of Structural Dynamics on Polarization Energies in Anthracene Single Crystals†. *J. Phys. Chem. C* **2010**, *114*, 20678−20685.
(27) Williams, M.; Tummala, N. R.; Aziz, S. G.; Risko, C.; Brédas, J.-L. Influence of Molecular Shape on Solid-State Packing in Disordered Pc61bm and Pc71bm Fullerenes. *J. Phys. Chem. Lett.* **2014**, *5*, 3427−3433.
(28) Tummala, N. R.; Mehraeen, S.; Fu, Y. T.; Risko, C.; Bredas, J. L. Materials-Scale Implications of Solvent and Temperature on [6,6]-Phenyl-C61-Butyric Acid Methyl Ester (PCBM): A Theoretical Perspective. *Adv. Funct. Mater.* **2013**, *23*, 5800−5813.
(29) Berendsen, H. J. C.; Vanderspoel, D.; Vandrunen, R. Gromacs - a Message Passing-Parallel Molecular-Dynamics Implementation. *Comput. Phys. Commun.* **1995**, *91*, 43−56.
(30) Hess, B.; Kutzner, C.; van der Spoel, D.; Lindahl, E. Gromacs 4: Algorithms for Highly Efficient, Load-Balanced, and Scalable Molecular Simulation. *J. Chem. Theory Comput.* **2008**, *4*, 435−447.
(31) Jorgensen, W. L.; Maxwell, D. S.; Tirado-Rives, J. Development and Testing of the OPLS All-Atom Force Field on Conformational Energetics and Properties of Organic Liquids. *J. Am. Chem. Soc.* **1996**, *118*, 11225−11236.
(32) Machui, F.; Abbott, S.; Waller, D.; Koppe, M.; Brabec, C. J. Determination of Solubility Parameters for Organic Semiconductor Formulations. *Macromol. Chem. Phys.* **2011**, *212*, 2159−2165.
(33) Machui, F.; Langner, S.; Zhu, X.; Abbott, S.; Brabec, C. J. Determination of the P3HT:PCBM Solubility Parameters Via a Binary Solvent Gradient Method: Impact of Solubility on the Photovoltaic Performance. *Sol. Energy Mater. Sol. Cells* **2012**, *100*, 138−146.
(34) Becke, A. D. Density-Functional Thermochemistry. V. Systematic Optimization of Exchange-Correlation Functionals. *J. Chem. Phys.* **1997**, *107*, 8554−8560.
(35) Grimme, S. Semiempirical Gga-Type Density Functional Constructed with a Long-Range Dispersion Correction. *J. Comput. Chem.* **2006**, *27*, 1787−1799.
(36) Körzdörfer, T.; Brédas, J.-L. Organic Electronic Materials: Recent Advances in the DFT Description of the Ground and Excited States Using Tuned Range-Separated Hybrid Functionals. *Acc. Chem. Res.* **2014**, *47*, 3284−3291.
(37) Baer, R.; Livshits, E.; Salzner, U. Tuned Range-Separated Hybrids in Density Functional Theory. *Annu. Rev. Phys. Chem.* **2010**, *61*, 85−109.
(38) Marenich, A. V.; Jerome, S. V.; Cramer, C. J.; Truhlar, D. G. Charge Model 5: An Extension of Hirshfeld Population Analysis for the Accurate Description of Molecular Interactions in Gaseous and Condensed Phases. *J. Chem. Theory Comput.* **2012**, *8*, 527−541.
(39) Wang, B.; Truhlar, D. G. Tuned and Balanced Redistributed Charge Scheme for Combined Quantum Mechanical and Molecular Mechanical (QM/Mm) Methods and Fragment Methods: Tuning Based on the Cm5 Charge Model. *J. Chem. Theory Comput.* **2013**, *9*, 1036−1042.
(40) Brédas, J.-L.; Beljonne, D.; Coropceanu, V.; Cornil, J. Charge-Transfer and Energy-Transfer Processes in Π-Conjugated Oligomers and Polymers: A Molecular Picture. *Chem. Rev.* **2004**, *104*, 4971−5004.
(41) Frisch, M. J.; Trucks, G. W.; Schlegel, H. B.; Scuseria, G. E.; Robb, M. A.; Cheeseman, J. R.; Montgomery, J. A., Jr.; Vreven, T.; Kudin, K. N.; Burant, J. C., et al. *Gaussian 09*, revision D.01, A.02; Gaussian, Inc.: Wallingford CT, 2009.
(42) Zhang, C.-R.; Coropceanu, V.; Sears, J. S.; Brédas, J.-L. Vibronic Coupling in the Ground State of Oligoacene Cations: The Performance of Range-Separated Hybrid Density Functionals. *J. Phys. Chem. C* **2014**, *118*, 154−158.
(43) Wang, X.-B.; Woo, H.-K.; Wang, L.-S. Vibrational Cooling in a Cold Ion Trap: Vibrationally Resolved Photoelectron Spectroscopy of Cold C60− Anions. *J. Chem. Phys.* **2005**, *123*, 051106.
(44) Wang, X.-B.; Woo, H.-K.; Huang, X.; Kappes, M. M.; Wang, L.-S. Direct Experimental Probe of the on-Site Coulomb Repulsion in the Doubly Charged Fullerene Anion C_{70}^{2-}. *Phys. Rev. Lett.* **2006**, *96*, 143002.
(45) Anthopoulos, T. D.; de Leeuw, D. M.; Cantatore, E.; van 't Hof, P.; Alma, J.; Hummelen, J. C. Solution Processible Organic Transistors and Circuits Based on a C70 Methanofullerene. *J. Appl. Phys.* **2005**, *98*, 054503.
(46) Körzdörfer, T.; Sears, J. S.; Sutton, C.; Brédas, J.-L. Long-Range Corrected Hybrid Functionals for Π-Conjugated Systems: Dependence of the Range-Separation Parameter on Conjugation Length. *J. Chem. Phys.* **2011**, *135*, 204107.
(47) Faber, C.; Janssen, J. L.; Côté, M.; Runge, E.; Blase, X. Electron-Phonon Coupling in the C60 Fullerene within the Many-Body Gw Approach. *Phys. Rev. B: Condens. Matter Mater. Phys.* **2011**, *84*, 155104.
(48) Yoshida, H. Low-Energy Inverse Photoemission Study on the Electron Affinities of Fullerene Derivatives for Organic Photovoltaic Cells. *J. Phys. Chem. C* **2014**, *118*, 24377−24382.

DOI: 10.1021/acs.jpclett.5b01709
J. Phys. Chem. Lett. 2015, 6, 3657−3662